Experimental Investigation of the ^{19}Ne(p,γ)^{20}Na Reaction Rate and Implications for Breakout from the Hot CNO Cycle

J. Belarge, S. A. Kuvin, L. T. Baby, J. Baker, I. Wiedenhöver, P. Höflich, A. Volya, J. C. Blackmon, C. M. Deibel, H. E. Gardiner, J. Lai, L. E. Linhardt, K. T. Macon, E. Need, B. C. Rasco, N. Quails, K. Colbert, D. L. Gay, and N. Keeley

Experimental investigation of the ^{19}Ne(p, γ)^{20}Na reaction rate and implications for breakout from the hot CNO cycle

J. Belarge,[1] S.A. Kuvin,[1] L.T. Baby,[1] J. Baker,[1] I. Wiedenhöver,[1] P. Höflich,[1] A. Volya,[1] J.C. Blackmon,[2] C.M. Deibel,[2] H.E. Gardiner,[2] J. Lai,[2] L.E. Linhardt,[2] K.T. Macon,[2] E. Need,[2] B.C. Rasco,[2] N. Quails,[3] K. Colbert,[3] D.L. Gay,[3] and N. Keeley[4]

[1]*Physics Department, Florida State University, Tallahassee, FL 32306*
[2]*Department of Physics and Astronomy, Louisiana State University, Baton Rouge, LA 70803*
[3]*Department of Physics, University of North Florida, Jacksonville, FL 32224, USA*
[4]*National Centre for Nuclear Research, ul. Andrzeja Sołtana 7, 05-400 Otwock, Poland*
(Dated: August 22, 2016)

Background: The ^{19}Ne(p, γ)^{20}Na reaction is the second step of a reaction chain which breaks out from the hot CNO-cycle, following the ^{15}O(α, γ)^{19}Ne reaction at the onset of X-ray burst events.

Purpose: We investigate the spectrum of the lowest proton-unbound states in ^{20}Na in an effort to resolve contradictions in spin-parity assignments and extract reliable information about the thermal reaction rate.

Method: The proton–transfer reaction ^{19}Ne(d, n)^{20}Na is measured with a beam of the radioactive isotope ^{19}Ne at an energy around the Coulomb-barrier and in inverse kinematics. The spectrum of protons emitted from the low-lying resonances is reconstructed and the transferred angular momentum analyzed.

Results: We observe three proton-resonances with the ^{19}Ne ground state, at 0.44 MeV, 0.66 MeV and 0.82 MeV c.m. energies, which are assigned 3^+, 1^+, and (0^+), respectively. In addition, we identify two resonances with the first excited state in ^{19}Ne, one at 0.20 MeV and one, tentatively, at 0.54 MeV. These observations allow us for the first time to experimentally quantify the astrophysical reaction rate on an excited nuclear state.

Conclusions: Our experiment shows an efficient path for thermal proton capture in ^{19}Ne(p, γ)^{20}Na, which proceeds through ground-state and excited-state capture in almost equal parts and eliminates the possibility for this reaction to create a bottleneck in the breakout from the hot CNO-cycle.

X-ray bursts are thermonuclear explosions in the atmosphere of a neutron star in a close binary system, where hydrogen– and helium–rich matter is accreted from the companion. Once the in-falling material reaches critical values for temperature and density, a transition occurs from hydrogen burning in the hot CNO-cycle to a thermonuclear runaway in the rapid proton-capture (rp–) process, which eventually reaches peak temperatures between 1-2 GK [1]. The nuclear reactions taking place in the transition to the rp-process therefore strongly influence the light curves of these events depending on the physical conditions of the accretion process. [1, 2]

Several studies have identified the ^{15}O(α, γ)^{19}Ne(p, γ)^{20}Na reaction chain as an important break-out path from the hot CNO-cycle, after which the rp-process can progress freely in a sequence of (p,γ) captures and β^+-decays. The importance of this path for the stability of the X-ray burst mechanism was discussed in more detail in Ref. [3], in light of a new upper limit for the ^{15}O(α, γ)^{19}Ne reaction rate [4]. The second reaction in this chain, ^{19}Ne(p, γ)^{20}Na, has also been the subject of numerous studies, but the relevant reaction rate remains uncertain within two orders of magnitude.

The most important open question is the unequivocal identification of the lowest-lying $l = 0, 1$ and 2 proton resonances between 0.2 and 0.5 MeV , inside the Gamow window for the breakout phase from the hot CNO-cycle. Several previous experimental works established that the

lowest resonance is located at 0.44 MeV center-of-mass (c.m.) energy, and the second one at 0.66 MeV [5–11]. Nevertheless, the assignments of spin and parity to these resonances remained contradictory, with the 0.44 MeV resonance either having been assigned 1^+ [5–8] or 3^+ [9, 11–13], and the 0.66 MeV resonance having been assigned values of (3^+) [5] 3,4 [6], 3^+ [7], (1^-) [9] or 3^-[12, 13]. Complicating matters further, some studies identified the lowest resonance at 0.44 MeV as a cross-shell "intruder" 1^+ state, which is expected around this energy as an isospin mirror to the 1_2^+ state at 3.172 MeV in ^{20}F. This hypothesis was proposed in Refs. [7, 8] and implies a resonance strength of one or two orders of magnitude smaller than the other possible assignments, thus potentially limiting the time-scale of the breakout from the hot CNO-cycle [8]. Additional weight was given to this argument when two experiments presented upper limits on the resonance strengths $\omega\gamma \leq 21$ meV [14] and $\omega\gamma \leq 15$ meV [15] from measurements of the (p,γ) proton capture cross section.

In order to clarify the proton-resonance structure in ^{20}Na, we conducted an experiment with the ^{19}Ne(d,n)^{20}Na(p)^{19}Ne reaction in inverse kinematics, using a beam of the radioactive isotope ^{19}Ne. To this end, a primary beam of ^{19}F at 117 MeV was produced at the John D. Fox Accelerator Laboratory of Florida State University, bombarding a Hydrogen–gas target contained between thin Havar windows and creating a secondary beam of recoiling ^{19}Ne particles by means of the (p,n) re-

action. The RESOLUT radioactive beam facility [16] was used to separate the recoiling ^{19}Ne particles in flight before focusing them onto the secondary target, a deuterated polyethylene (CD$_2$) foil with a thickness of 0.52 mg/cm^2. The ^{19}Ne beam of ∼1700 particles per second at 86 MeV energy constituted 13% of the beam composition. The main contaminants were ^{19}F primary beam particles, multiple–scattered in the production target windows.

The ^{19}Ne(d, n)^{20}Na reaction used in our experiment has favorable conditions for the population of the low-angular momentum resonances of astrophysical importance in ^{20}Na. For its interpretation, we can also rely on experimental data from the isospin-mirror reaction ^{19}F(d, p)^{20}F. The available data, e.g. from Ref. [17] and shell-model calculations, e.g. with the usd-a interaction [18] allow us to predict which states will be populated with significant cross sections,namely the 1_2^+, 3_3^+, 0_1^+ and the 3_4^+ state.

Our experiment populated the resonances via the ^{19}Ne(d, n)^{20}Na reaction and detected the ^{20}Na$^* \rightarrow ^{19}$Ne + p decay path, which was used to reconstruct the proton–resonance spectrum in ^{20}Na. The compact detection system consisted of thin (65 μm) and thick (500 μm) annular double-sided silicon strip detectors (DSSD) covering angles in the laboratory frame from 8–21 degrees for detection of protons, and a position-resolving ion chamber capable of detecting the heavy-ion reaction products alongside the unreacted beam particles. The protons and ^{19}Ne particles of interest were selected according to their characteristic energy losses. In addition, we required a time-of-flight characteristic of the ^{19}Ne beam particles by measuring the time of proton detection relative to accelerator-RF reference, in effect suppressing events from the contaminant beam components.

The proton c.m. energies were reconstructed from the energies and angles of the protons and ^{19}Ne particles. The resulting spectrum is presented in Fig. 1. We fitted the spectrum with Gaussian peaks at the known resonance energies, keeping the width fixed to values extracted from a Monte-Carlo simulation of the experimental setup. A polynomial background was added by fitting the spectrum at higher energies. From the peak areas, the beam intensity, the target thickness and the simulated detector efficiency, the cross sections were determined. Five peak structures were analyzed, at 0.20 MeV with $5.5\,^{\pm 0.7\,\mathrm{stat}}_{\pm 0.4\,\mathrm{sys}}$mbarn, at 0.44 MeV with $5.8^{\pm 0.7\,\mathrm{stat}}_{\pm 1.8\,\mathrm{sys}}$mbarn, at 0.54 MeV with $10\,^{\pm 2\,\mathrm{stat}}_{\pm 6\,\mathrm{sys}}$, at 0.66 MeV with $47\,^{\pm 2\,\mathrm{stat}}_{\pm 7\,\mathrm{sys}}$ mbarn and at 0.82 MeV, with $5.2^{\pm 0.9\,\mathrm{stat}}_{\pm 1.0\,\mathrm{sys}}$ mbarn. The systematic errors subsume the uncertainties of the target thickness, the detector geometry and the number of incoming beam particles. We identify the 0.66 MeV peak with the 2.849 MeV state, the 0.44 MeV peak with the 2.645 MeV state and the

0.82 MeV peak with the 3.060 MeV state. No state corresponding to the 0.20 MeV peak or the 0.54 MeV peak were previously observed. Based on arguments given in the following paragraphs, we interpret the 0.20 MeV peak as protons emitted from the 0.44 MeV resonance populating the $5/2^+$ first excited state in ^{19}Ne at 0.238 MeV excitation. The events around 0.54 MeV most likely represent protons from the 2.972 MeV observed in [5, 7, 8, 19] populating the ^{19}Ne excited state as well.
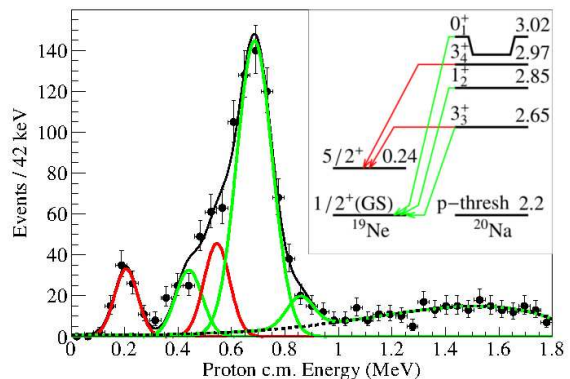

FIG. 1. Proton c.m. energy spectrum for ^{19}Ne(d,n)^{20}Na(p) events. Five structures are extracted, at energies 0.20 MeV, 0.44 MeV, 0.54 MeV, 0.66 MeV and 0.82 MeV. The overall fit, displayed in black, is a sum of a polynomial background (black dotted line), and the Gaussian peaks.

The analysis of angular distributions for single-nucleon transfer reactions, such as (d,n), is a reliable method to determine the angular momentum of the populated nuclear states. The l-value of the transferred proton can be determined by a comparison of the neutron angular distribution to a calculation of the reaction mechanism. We applied a technique to analyze the neutron angular distribution through the energies of the charged reaction products, similar to a method described in Ref.[20].

Since the neutron is the only final-state particle not detected experimentally, we can reconstruct the missing neutron energy from the energy balance of our events. Furthermore, for a given resonance energy, the neutron energy exhibits a rapid kinematic variation as a function of the emission angle, which creates an imprint of the neutron angular distribution in the summed energies of the detected particles. The functional relation between these summed energies and the c.m. neutron-angles is expressed through the secondary x-axis of Figs. 2 and 3.

In order to obtain a quantitative model of the reaction mechanism, calculations of a Coupled-Channel Born Approximation (CCBA) formalism were performed using the code FRESCO [21] and an approach similar to that described in Ref. [22]. We applied a "weak" binding approximation, which is justified by the small widths of the resonances involved. We analyzed the distributions of the

summed proton and ^{19}Ne energies for the events from the 0.20 and 0.66 MeV peaks. The 0.44 MeV, 0.54 MeV and 0.82 MeV peaks could not be analyzed independently, because of their proximity to the larger 0.66 MeV peak. Fig. 2 shows the distribution obtained for the 0.66 MeV resonance. The energy resolution of the ion chamber spectrum was determined to be 2.5 MeV FWHM from the energies observed for the beam particle detected after passing through the secondary target foil. The angular distributions of the CCBA calculation for different l hypotheses were translated to the summed proton– and ^{19}Ne energies through a Monte-Carlo simulation.

The comparison of the experimental distribution to the hypotheses results in a reduced $\chi^2 = 3.5$ for $l = 0$, and $\chi^2 = 5.1$ for $l = 2$. We thus identify the 0.66 MeV resonance with the known 2.849 MeV state in ^{20}Na and assign it spin and parity 1^+. The CCBA calculation also allowed us to determine a proton $l = 0$ spectroscopic factor of $C^2S = 0.26 \, ^{\pm 0.01 \, \text{stat}}_{\pm 0.04 \, \text{sys}}$ for the 1^+ state at 2.849 MeV.
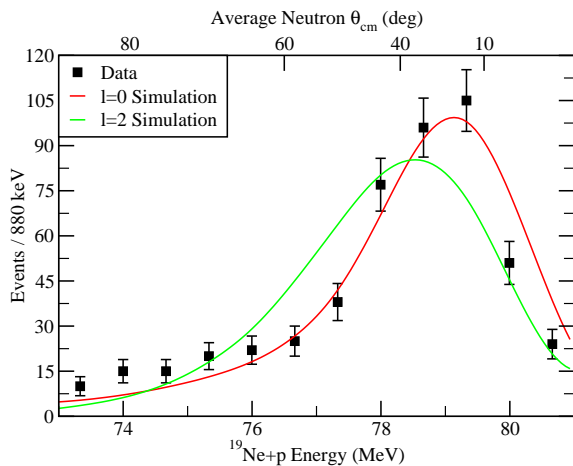

FIG. 2. ^{19}Ne+p energy spectrum for 0.66 MeV peak. The experimental data are compared to the results of a Monte-Carlo simulation based on an angular distribution from CCBA calculations for $l = 0$ and $l = 2$. The energy resolution in this distribution was determined to be 2.5 MeV FWHM.

The same analysis was performed on the events in the 0.20 MeV peak, which is displayed in Fig. 3. Here, the distribution fits an $l = 2$ hypothesis with a reduced χ^2=1.8, compared to χ^2=4.3 for $l = 0$. The match with $l = 2$ is evident both through the greater width and the lower centroid of the distribution as compared to the 0.66 MeV resonance. If the 0.20 MeV peak was hypothetically interpreted as an isolated $l = 2$ resonance, it would decay by γ-emission, with an expected proton-decay width one order of magnitude smaller than typical γ-decay widths. This hypothesis is in contradiction with the observed proton decay, and we therefore interpret the 0.20 MeV and 0.44 MeV peaks as two proton–decay branches stemming from the same resonance at 0.44 MeV. Note that this analysis was used to assign $l = 2$
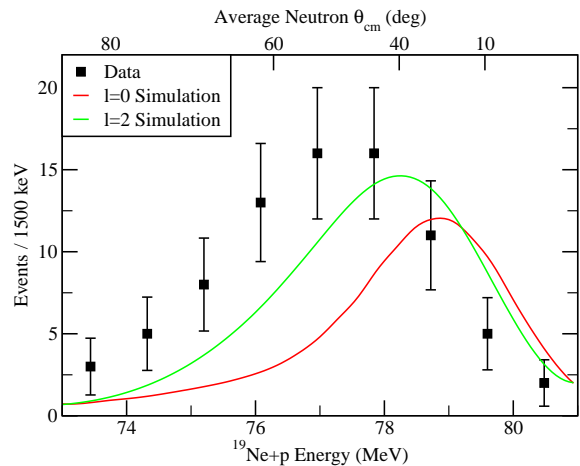

FIG. 3. Same as Fig.2, only selected on the 0.20 MeV peak. The simulated distributions assume the population of the 0.238 MeV first excited state in ^{19}Ne.

character to the (d,n) angular distribution, although it was observed through the $l = 0$ proton-decay branch.

The combined experimental cross section of the 0.20 MeV and 0.44 MeV peaks is 11.3 $^{\pm 1.1 \, \text{stat}}_{\pm 1.8 \, \text{sys}}$ mbarn , with a branching fraction of 51% $^{\pm 4 \, \text{stat}}_{\pm 8 \, \text{sys}}$ to the ground state in ^{19}Ne. The $l = 2$ nature of the transfer reaction leads us to assign spin and parity 3^+ to this resonance. We use the observed proton branching and a barrier-penetration model to deduce the ratio of the spectroscopic factors for both proton-branches. Both are then adjusted by a common factor to reproduce the absolute experimental cross section. We extract a spectroscopic factor $C^2S = 0.50^{\pm 0.06}_{\pm 0.03}$ relative to the $5/2^+$ ^{19}Ne first excited state and $C^2S = 0.07 \, ^{\pm 0.01}_{\pm 0.02}$ relative to the $1/2^+$ ^{19}Ne ground state.

Table I lists the spectroscopic factors obtained from our analysis and compares them to those extracted from the isospin-mirror reaction ^{19}F(d, p)^{20}F [17]. The good agreement for the 0.66 MeV and 0.44 MeV resonances in ^{20}Na lends additional support to our assignment of spins and parities. In addition, we tentatively identify the 2.972 resonance as the mirror-partner to the 3.59 MeV (3^+) state in ^{20}F, which is the only remaining ^{20}F state in the excitation region to be populated strongly in ^{19}F(d, p)^{20}F [17]. The spectroscopic factor extracted for the 0.82 MeV resonance is consistent with the one expected for the 0^+ state, but in absence of an angular distribution analysis, no firm assignment is given.

A shell model calculation with the usd-a interaction [18] was used to predict the respective spectroscopic factors, which are also listed in Table I. A striking feature in the shell model, and of our experiment, is the strong connection between the 3_3^+ proton resonance and the first excited state in ^{19}Ne. The tentative identification of the experimental 2.972 MeV state with the 3_4^+ shell model excitation and the 3.59 MeV state in ^{20}F is a plausible

TABLE I. Properties of low-lying resonances in ^{19}Ne + p (see text). The fourth column specifies the resonance wave-function, either relative to the $1/2^+$ ^{19}Ne ground state or the 0.238 MeV $5/2^+$ ^{19}Ne first excited state.

E_{ex} (MeV)	J^π	E_{res}(c.m.) (MeV)	Resonance $p\times^{19}$Ne	$\sigma\,^{\rm stat}_{\rm sys}$ (mbarn)	Branch $^{\rm stat}_{\rm sys}$ (%)	$C^2S\,^{\rm stat}_{\rm sys}$	C^2S_{mirror}	C^2S_{SM}	$\Gamma_p\,^{\rm stat}_{\rm sys}$ (meV)	Γ_γ (meV)	$\omega\gamma\,^{\rm stat}_{\rm sys}$ (meV)
2.645	3_3^+	0.20	$(l=0)\times 5/2^{+\rm a}$	$5.5\,^{\pm0.7}_{\pm0.4}$	$49\,^{\pm4}_{\pm8}$	$0.50^{\pm0.06}_{\pm0.03}$		0.29	$584\,^{+66}_{+36}$	$82\,^{\pm18}_{\pm22}$	$23\,^{\pm5}_{\pm6}$
2.645	3_3^+	0.44	$(l=2)\times 1/2^+$	$5.8\,^{\pm0.7}_{\pm1.8}$	$51\,^{\pm4}_{\pm8}$	$0.07\,^{\pm0.01}_{\pm0.02}$	0.05	0.03	$615\,^{+62}_{+259}$	$82\,^{\pm18}_{\pm22}$	$74\,^{+15}_{+17}$
2.849	1_2^+	0.66	$(l=0)\times 1/2^+$	$47\,^{\pm2}_{\pm7}$	100	$0.26\,^{\pm0.01}_{\pm0.04}$	0.40	0.47	$4.40\rm e6\,^{+2e5}_{+6e5}$	$28\,^{+3}_{\pm10}$	$21\,^{\pm2}_{\pm6}$
2.972	(3_4^+)	0.54	$(l=0)\times 5/2^{+\rm a}$	$10^{\pm2}_{\pm6}$	100			0.25		(82)	(48)
2.972	(3_4^+)	0.77	$(l=2)\times 1/2^+$			$0.05^{\pm0.01}_{\pm0.03}$	0.05	0.02			
3.060	(0_1^+)	0.82	$(l=0)\times 1/2^+$	$5.2\,^{\pm0.9}_{\pm1.0}$	100	$0.27\,^{\pm0.05}_{\pm0.05}$	0.28	0.58	$1.19\rm e7\,^{+2e6}_{+2e6}$	$66\,^{+7}_{\pm15}$	$17\,^{+3}_{\pm5}$

$^{\rm a}$ Resonance with the ^{19}Ne first excited state

interpretation, consistent with a sufficiently large spectroscopic factor to be observable in our experiment. The shell-model wave functions predict a proton-branching ratio of 98.9% towards the first excited state in ^{19}Ne, also consistent with our observations.

The present determination of the resonance spectrum in ^{20}Na has a large impact on the ^{19}Ne(p,γ)^{20}Na astrophysical reaction rate. Owing to their relatively high energies, the 1_2^+, (3_4^+) and (0_1^+) resonances will not significantly contribute to the ^{19}Ne(p,γ)^{20}Na capture reaction in astrophysical environments. Rather, the reaction rate will be dominated by capture to the lowest resonance at 0.44 MeV c.m. energy. The 3_3^+ assignment to this resonance allows us to calculate the Γ_γ decay width from information obtained for the 3_3^+ state in the mirror nucleus ^{20}F. The most precise measurement to date reports the level lifetime as 5.2 $\pm$1.1 fs [23]. By applying the γ–matrix elements to the analog ^{20}Na transitions, we deduce a $\Gamma_\gamma = 82^{\pm18\,\rm stat}_{\pm22\,\rm sys}$ meV.

The proton-widths of the two observed decays of the 3_3^+, based on the CCBA analysis of the experimental cross section and the branching ratio, are Γ_{p0}=$615^{\pm62\,\rm stat}_{\pm259\,\rm sys}$ meV and Γ_{p1}= $584^{\pm66\,\rm stat}_{\pm36\,\rm sys}$ meV.

From these widths the resonance strengths are calculated as

$$\omega\gamma = \frac{2J+1}{2(2j+1)}\frac{\Gamma_\gamma\Gamma_p}{\Gamma_{total}} \quad (1)$$

where J is the spin of the populated resonance, here 3, and j is the ^{19}Ne spin, 1/2 or 5/2. We extract $\omega\gamma = $ 69 meV for proton-capture on the ^{19}Ne ground state and $\omega\gamma = $ 21 meV for capture on the 0.238 keV excited state. From here, the averaged thermal nuclear reaction rates are calculated by the expression

$$N_A\langle\sigma v\rangle = N_A\left(\frac{2\pi}{\mu kT}\right)^{3/2}\hbar^2\omega\gamma\exp(-E_{c.m.}/kT), \quad (2)$$

where the c.m. resonance energy enters as a Boltzmann-factor, stemming from the thermal energy distribution of the protons.

The possibility of excited-state proton capture for the present reaction has been discussed in Ref. [14], where

it was predicted for the 0.66 MeV resonance, based on the authors' 3^+ assignment and the corresponding shell-model predictions. Our experiment allows us for the first time to quantify excited-state proton capture based on experimental information. The 0.44 MeV resonance represents an unusual case, as it exhibits two proton channels of nearly equal decay widths, which allows for a significant contribution from proton capture on the first excited state. Although the thermal population of the first excited state in ^{19}Ne is relatively small and remains below a few percent up to temperatures of 1 GK, this suppression is completely overcome by the enhancement stemming from the lower resonance energy of 0.20 MeV. An estimate based on a detailed–balance condition for the ^{19}Ne first–excited state with 18.0 nsec lifetime [24] shows the equilibration rate to be much faster than the (p,γ) reaction rate at all temperatures, providing justification for the argument given above.

The resulting thermal reaction rates are displayed in Panel (a) of Fig. 4, which show that proton capture in the 0.44 MeV 3_3^+ resonance is dominant, with nearly equal contributions from capture on the ^{19}Ne ground state and the first excited state. In this result the excited state thermal population was taken into account, which remains below a few percent over the displayed temperature range. The reaction rate for the tentatively identified (3_4^+) was estimated using the Γ_γ value of the 3_3^+ for want of specific experimental data. Panel (b) of Fig. 4 displays a comparison between the reaction rate obtained from our work with the rates from Vancraeynest et al. [14], where the experimental upper limit of the (p,γ) strength was used. Also displayed is the rate from Smith et al. [8], an upper limit extracted from the assignment of the 1^+ intruder configuration to the 0.44 MeV resonance. Our experiment rules out this interpretation, but also contradicts the upper limits of (p,γ) resonance strengths measured in the works of Refs. [14] and [15].

In summary, we investigated the resonance spectrum in ^{19}Ne+p by means of the ^{19}Ne(d,n)^{20}Na(p) reaction with a radioactive beam of ^{19}Ne. We identified the 3^+ and 1^+ resonances, which dominate the astrophysical reaction rate and we showed that proton-capture rate on
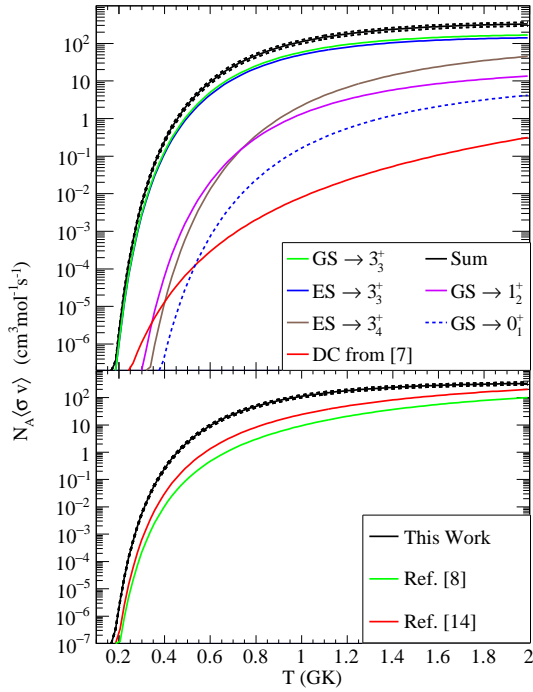
FIG. 4. Panel (a) ^{19}Ne(p,γ)^{20}Na–reaction rates calculated with the resonance parameters obtained in this work, labeled "GS" for ground-state and "ES" for excited-state resoances. Panel (b) Total reaction rates from this work compared to upper limits obtained by Vancraeynest *et al.* [14] and Smith *et al.* [8]. The error limits (dashed lines) on the total reaction rate are ±32%, stemming mainly from the uncertainty in the Γ_γ value of the 0.44 MeV resonance.

an excited state leads to the second largest contributing term in the overall rate. In effect, the extracted thermal rate for the ^{19}Ne(p,γ)^{20}Na reaction is higher than deduced in previous investigations and significantly higher than the reaction rate (Ref. [3]) of ^{15}O(α,γ)^{19}Ne, which precedes it during the breakout from the hot CNO-cycle. Based on these properties, the ^{19}Ne(p,γ)^{20}Na reaction does not constitute a bottleneck in the break-out phase from the hot CNO cycle.

[1] H. Schatz and K. E. Rehm, Nuclear Physics A **777**, 601 (2006), special Issue on Nuclear Astrophysics.
[2] H. Schatz, L. Lars Bildsten, A. Cumming, and M. Wiescher, The Astrophysical Journal **524**, 1014 (1999).
[3] J. L. Fisker, W. Tan, J. Görres, M. Wiescher, and R. L. Cooper, The Astrophysical Journal **665**, 637 (2007).
[4] W. P. Tan, J. Görres, J. Daly, M. Couder, A. Couture, H. Y. Lee, E. Stech, E. Strandberg, C. Ugalde, and M. Wiescher, Phys. Rev. C **72**, 041302 (2005).
[5] S. Kubono, H. Orihara, S. Kato, and T. Kajino, The Astrophysical Journal **344** (1989).
[6] N. Clarke, P. Hayes, M. Becha, C. Pinder, and S. Roman, J.Phys.G:Nucl.Part.Phys. **16**, 1547 (1990).
[7] L. Lamm, C. Browne, J. Görres, S. Graff, M. Wiescher, A. Rollefson, and B. Brown, Nuclear Physics A **510**, 503 (1990).
[8] M. Smith, P. Magnus, K. Hahn, A. J. Howard, and P. Parker, Nuclear Physics A **536**, 333 (1992).
[9] N. Clarke, S. Roman, C. Pinder, and P. Hayes, J.Phys.G:Nucl. Part. Phys. **19**, 1411 (1993).
[10] B. D. Anderson, N. Tamimi, A. R. Baldwin, M. Elaasar, R. Madey, D. M. Manley, M. Mostajabodda'vati, J. W. Watson, W. M. Zhang, and C. C. Foster, Phys. Rev. C **43**, 50 (1991).
[11] B. D. Anderson, B. Wetmore, A. R. Baldwin, L. A. C. Garcia, D. M. Manley, R. Madey, J. W. Watson, W. M. Zhang, B. A. Brown, C. C. Foster, and Y. Wang, Phys. Rev. C **52**, 2210 (1995).
[12] B. A. Brown, A. E. Champagne, H. T. Fortune, and R. Sherr, Phys. Rev. C **48**, 1456 (1993).
[13] J. P. Wallace and P. J. Woods, Phys. Rev. C **86**, 068801 (2012).
[14] G. Vancraeynest, P. Decrock, M. Gaelens, M. Huyse, P. Van Duppen, C. R. Bain, T. Davinson, R. D. Page, A. C. Shotter, P. J. Woods, F. Binon, P. Duhamel, J. Vanhorenbeeck, R. Coszach, T. Delbar, W. Galster, J. S. Graulich, P. Leleux, E. Liénard, P. Lipnik, C. Michotte, A. Ninane, J. Vervier, H. Herndl, H. Oberhummer, C. Sükösd, and M. Wiescher, Phys. Rev. C **57**, 2711 (1998).
[15] M. Couder, C. Angulo, E. Casarejos, P. Demaret, P. Leleux, and F. Vanderbist, Phys. Rev. C **69**, 022801 (2004).
[16] I. Wiedenhöver, L. Baby, D. Santiago-Gonzalez, A. Rojas, J. Blackmon, G. Rogachev, J. Belarge, E. Koshchiy, A. Kuchera, L. Linhardt, J. Lai, K. Macon, M. Matos, and B. Rascol, Proceedings of the 5th International Conference on "Fission and properties of neutron-rich nuclei" (ICFN5) , 144 (2014).
[17] H. T. Fortune and R. R. Betts, Phys. Rev. C **10**, 1292 (1974).
[18] W. A. Richter, S. Mkhize, and B. A. Brown, Phys. Rev. C **78**, 064302 (2008).
[19] J. Wallace, P. Woods, G. Lotay, A. Alharbi, A. Banu, H. David, T. Davinson, M. McCleskey, B. Roeder, E. Simmons, A. Spiridon, L. Trache, and R. Tribble, Physics Letters B **712**, 59 (2012).
[20] A. S. Adekola, C. R. Brune, D. W. Bardayan, J. C. Blackmon, K. Y. Chae, J. A. Cizewski, K. L. Jones, R. L. Kozub, T. N. Massey, C. D. Nesaraja, S. D. Pain, J. F. Shriner, M. S. Smith, and J. S. Thomas, Phys. Rev. C **85**, 037601 (2012).
[21] I. J. Thompson, Computer Physics Reports **7**, 167 (1988).
[22] N. Keeley, N. Alamanos, and V. Lapoux, Phys. Rev. C **69**, 064604 (2004).
[23] S. Raman, E. K. Warburton, J. W. Starner, E. T. Jurney, J. E. Lynn, P. Tikkanen, and J. Keinonen, Phys. Rev. C **53**, 616 (1996).
[24] J. A. Becker, J. W. Olness, and D. H. Wilkinson, Phys. Rev. **155**, 1089 (1967).